A Current-Mode Control Technique with Instantaneous Inductor-Current Feedback for UPS Inverters

Hongying Wu*, Dong Lin*, Dehua Zhang*, Kaiwei Yao**, and Jinfa Zhang*

*Department of Electrical Engineering, Zhejiang University, Hangzhou 310027, P. R. China
**Hwadar Electronics Co., Ltd., Shenzhen 518067, P. R. China

***Abstract*-A current-mode control technique with output filter inductor-current instantaneously controlled is proposed for voltage-source inverter of uninterruptible power supplies (UPS's). This technique shows good dynamic responsibility, high stability and current limiting in case of load short. Small-signal analysis, parameter design, simulation and experimental results are given in this paper.**

I. Introduction

For Uninterruptible Power Supply (UPS) inverters, it is important to have high stability and reliability as well as fast dynamic responsibility particularly under nonlinear loads such as computers. The control technique used is one of the most significant factors affecting the whole performance of the system. Sine pulse width modulation (SPWM) technique is preferred to obtain a sinusoidal output-voltage for the reason of simple control scheme and easy control of the harmonic content in the output-voltage. The traditional average voltage feedback SPWM control only regulates the amplitude of the output-voltage with the waveform open-loop controlled, showing very slow dynamic response to load disturbance and poor waveform under nonlinear loads [1]. So instantaneous voltage feedback SPWM control techniques have been developed and widely used in the past years [2]. The waveform of the output is instantaneously regulated by the comparison of the instantaneous voltage feedback with a sinusoidal reference. The influence of component nonlinear characteristics and dc voltage fluctuation is restrained. Dynamic performance is greatly improved, but still not good enough for rush current and nonlinear load because only single voltage-mode control is used. Furthermore, the difficulty of the system stability design is raised.

To overcome these drawbacks, current-mode control techniques were developed and have been verified to be effective in improving the system stability and dynamic responsibility [1], [3]. Current-mode control is basically a multiple-loop control method in which the current negative-feedback loop is commanded by the error signal of the outer voltage regulation loop. In terms of the typical current-mode control techniques, hysteresis current control, predictive current control and SPWM current control have been reported. Hysteresis current control has a fast transient response, but the switching frequency varies widely [4]. So a variety of improved constant-frequency hysteresis current control techniques were proposed with additional circuits for adaptive hysteresis band [5]–[8]. To reduce the complication, most of them are implemented by digital techniques. Thus switching frequency is limited by operation and D/A or A/D time, which can not well satisfy the requirement of size reducing and fast dynamic response of UPS. Predictive current control requires a good knowledge of load parameters, in addition to having the same calculation problem [8], [9]. In contrast, SPWM current control, with comparison of instantaneous current error with triangular waveform, not only maintains constant switching frequency but also provides fast dynamic response for UPS application. Meanwhile, the control circuit is relatively simple. Some of SPWM current control techniques with regulation of filter capacitor-current for LC filter-VSI inverters were proposed in [10], [11]. The output-voltage is differentially pre-rectified by the control of capacitor current. The sensitivity to parameter variations is reduced and the robustness is much improved. Furthermore, the scheme has very fast dynamic response in both linear and nonlinear load applications.

In this paper a SPWM current-mode control technique with filter inductor-current instantaneously controlled is proposed. The current in the inductor includes both filter capacitor current and load current. So the differential pre-rectification is retained and the load current can be closely controlled, which contribute to the fast dynamic response, high stability and current-limiting in case of load short as well as easy load sharing for parallel operation of UPS systems [12].

II. Operation Of The Proposed Control Technique

The control diagram of the proposed current-mode control technique on a LC-filter inverter is shown in Fig. 1. A single-phase half-bridge structure is used for clear and convenient discussion. S1 & S2 are switches, Ed+ & Ed- are dc supplies, and L & C are inductor & capacitor that compose the output filter. Multiple-loop control is necessary in this control method. The voltage control loop acts as the outer loop. The output-voltage feedback is compared with a sine

0-7803-5160-6/99/$10.00 © 1999 IEEE.

reference signal and the error voltage is compensated by a PI-regulator to produce the current reference i_{ref}. The proposed instantaneous current control loop acts as the inner loop. The switching current through the inductor is sensed and compared with i_{ref}. After compensated by a P-regulator, the error signal v_{er} is compared with a triangular waveform v_t to generate SPWM signal for switching control of S1 & S2.

The switching control operation is represented in Fig. 2 (supposing that the gain of the P-regulator equals 1). The operation of the current control loop is equivalent to a comparison of the inductor-current feedback i_L and the equivalent reference $\underline{i_{ref}+v_t}$. S1 keeps on and S2 keeps off as i_L is less than $\underline{i_{ref}+v_t}$, and i_L increases. As i_L reaches the values higher than $\underline{i_{ref}+v_t}$, S1 turns off, S2 turns on, and i_L decreases. It can be seen that as long as the slope of the inductor-current is kept less than that of the triangular waveform, the SPWM switching signal can be carried out and the high frequency ripples of the inductor-current can be limited in a window decided by the triangular waveform.

III. Stability Analysis

With small-signal averaging model, the control block can be obtained as shown in Fig. 3 (supposing resistant load for simplicity). The definition of the parameters in Fig. 3 are listed in TABLE I.

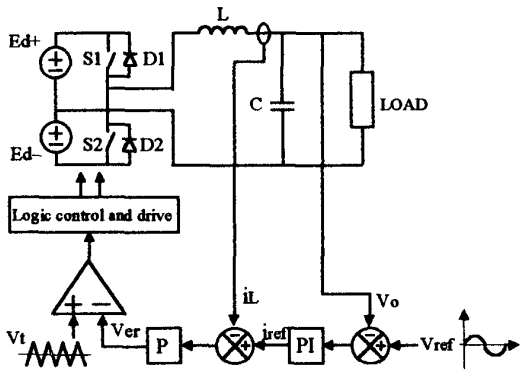

Fig. 1. Control diagram of the proposed control technique

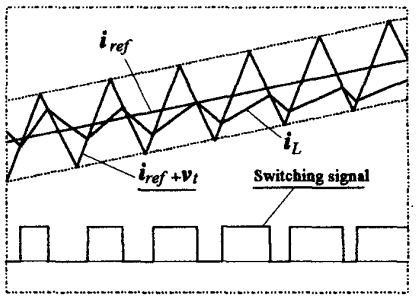

Fig. 2. The operation of the proposed current control

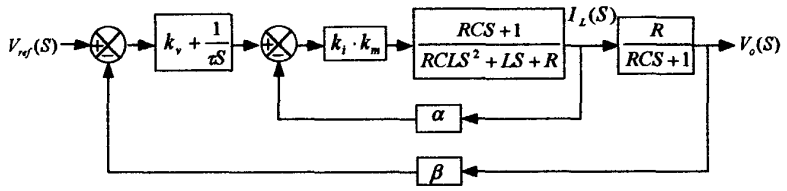

Fig. 3. Block diagram of the proposed method

TABLE I

Definition Of The Parameters In Fig. 3

R	Load Resistance
α	Gain Of The Inductor-Current Feedback
β	Gain Of The Output-voltage Feedback
$k_v+\frac{1}{\tau S}$	Transfer Function Of The PI-Regulator
k_i	Gain Of The P-Regulator
k_m	Gain Of The Effective SPWM Amplifier
$\frac{RCS+1}{RLCS^2+LS+R}$	Admittance Of The Output Filter And Load
$\frac{R}{RCS+1}$	Impedance Of The Filter Capacitor And Load

The transfer functions can be derived as:

• Open-loop transfer function of the system

$$G_o = \frac{\beta k_i k_m R}{\tau} \cdot \frac{k_v \tau S + 1}{S[RLCS^2 + (L + \alpha k_i k_m RC)S + R + \alpha k_i k_m]}, \quad (1)$$

• Closed-loop transfer function of the system

$$G_c = \frac{V_o(s)}{V_{ref}(s)} = \frac{k_i k_m R(k_v \tau S + 1)}{RLC\tau S^3 + (L + \alpha k_i k_m RC)\tau S^2 + (R + \alpha k_i k_m + \beta k_i k_m k_v R)\tau S + \beta k_i k_m R}. \quad (2)$$

Equation (1) can be re-written as

$$G_o(S) = \frac{\beta k_i k_m k_v}{LC} \cdot \frac{S + \frac{1}{k_v \tau}}{S[S^2 + (\frac{1}{RC} + \frac{\alpha k_i k_m}{L})S + \frac{1}{LC} + \frac{\alpha k_i k_m}{RLC}]}, \quad (3)$$

Then the open-loop zeros and poles are determined:

$$S_Z = -\frac{1}{k_v \tau},$$

$$S_{p1} = 0,$$

$$S_{p2,3} = \frac{1}{2}\left[-(\frac{1}{RC} + \frac{\alpha k_i k_m}{L}) \pm \sqrt{(\frac{1}{RC} - \frac{\alpha k_i k_m}{L})^2 - \frac{4}{LC}}\right].$$

Here, $S_{p2,3}$ are negative reals under the conditions that $R > \frac{L}{\alpha k_i k_m C - 2\sqrt{LC}}$ and $\alpha k_i k_m > 2\sqrt{L/C}$. Such conditions can always be satisfied under an appropriate design. Then the root-loci of the closed-loop system under different load conditions can be drawn as Fig. 4. It can be seen from the figure that the system has stable closed-loop poles under any condition. The asymptote of the loci is parallel to the imaginary axis, and the intersecting point of the asymptote with the real axis lies on $\sigma_a = -\frac{1}{2}(\frac{1}{RC} + \frac{\alpha k_i k_m}{L} - \frac{1}{k_v \tau})$. The asymptote will go nearer to the imaginary axis as R increases. But since commonly $\frac{1}{RC} << \frac{\alpha k_i k_m}{L}$ and $\frac{1}{k_v \tau} << \frac{\alpha k_i k_m}{L}$, the effect of R is not significant and the loci can stay far away from the imaginary axis, which contributes to short regulating time and small over-regulating magnitude.

If the situation $R < \frac{L}{\alpha k_i k_m C - 2\sqrt{LC}}$ while $\alpha k_i k_m > 2\sqrt{L/C}$ appears in case of heavy load, $S_{p2,3}$ will become conjugate complexes with negative real parts. The root-loci of the closed-loop system will transmute to Fig. 5. The asymptote is still far from the imaginary axis and the system will maintain good performance.

Since S_{p1} is very close to S_Z, the system can be simplified as 2nd-order system. Equation (3) turns to be

$$G_o(S) = \frac{\beta k_i k_m k_v}{LC} \cdot \frac{1}{S^2 + (\frac{1}{RC} + \frac{\alpha k_i k_m}{L})S + \frac{1}{LC} + \frac{\alpha k_i k_m}{RLC}}. \quad (4)$$

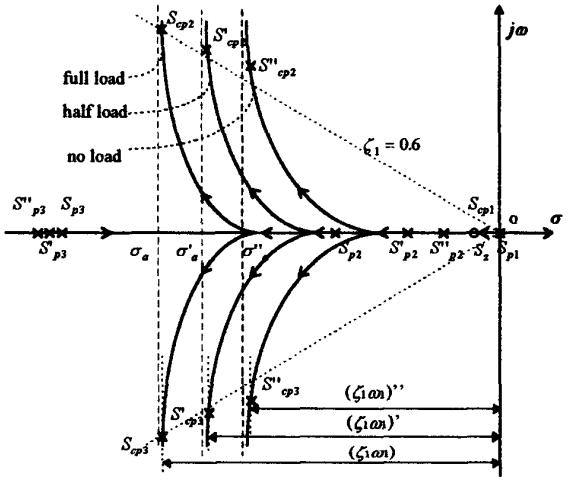

S_{p1}: open-loop, any load
S_{p2}, S_{p3}: open-loop, full load
S'_{p2}, S'_{p3}: open-loop, half load
S''_{p2}, S''_{p3}: open-loop, no load
S_{cp1}: closed-loop, any load
S_{cp2}, S_{cp3}: closed-loop, full load
S'_{cp2}, S'_{cp3}: closed-loop, half load
S''_{cp2}, S''_{cp3}: closed-loop, no load

Fig. 4. Root-loci of the closed-loop system (with real poles)

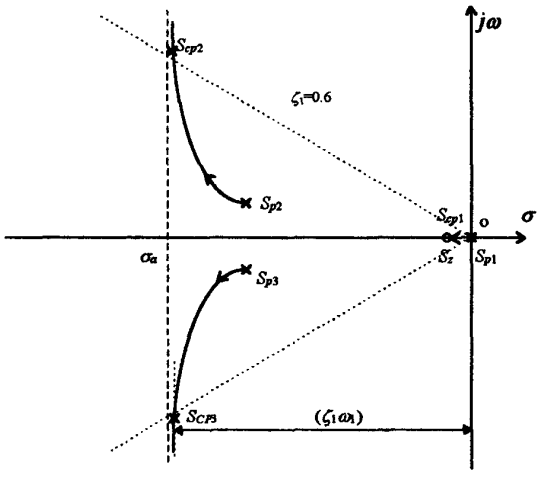

Fig. 5. Root-loci of the closed-loop system (with two complex poles)

That is

$$G_{or}(S)=\frac{K}{\tau_1^2 S^2+2\zeta_1\tau_1 S+1}, \tag{5}$$

where,

$$K=\frac{\beta k_i k_m k_v}{1+\frac{\alpha k_i k_m}{R}}, \tag{6}$$

$$\tau_1=\sqrt{\frac{RLC}{R+\alpha k_i k_m}}, \tag{7}$$

$$\zeta_1=\frac{(\frac{1}{RC}+\frac{\alpha k_i k_m}{L})\sqrt{RCL}}{2\sqrt{R+\alpha k_i k_m}}. \tag{8}$$

The simplified system is a combination of a proportional unit and a 2nd-order resonant unit. The damping coefficient ζ_1 and the regulating time t_s (proportional to $\frac{1}{\zeta_1\omega_1}=\frac{2}{\frac{1}{RC}+\frac{\alpha k_i k_m}{L}}$, noting $\omega_1=\frac{1}{\tau_1}$) are less dependent on the load especially under light load. Fig. 6 shows the magnitude and phase responses of (5). The phase margin is large enough for stability consideration.

IV. Parameter Design

LC-filter is designed according to the permissible maximum output-voltage ripple and the switching frequency. The high frequency current through the filter also needs to be limited in order to reduce the loss and EMI (Electro-Magnetic Interference). Because the largest high frequency inductor-current ripples are around zero output-voltage and the output-voltage ripples are relevant directly with the inductor-current ripples, zero output-voltage condition is used to design L and C. Combining

$$\Delta I_{Lm}<\frac{E_d}{2L\cdot f_{SW}} \tag{9}$$

and

$$\Delta V_{om}<\frac{E_d}{4\pi f_{SW}^2\cdot LC} \tag{10}$$

yields the determination of L and C.

Under current-mode control, parameter design of control loop is focused on the inner loop. The voltage feedback controller can be designed conventionally, while the current feedback controller should be designed carefully for the reliable comparison of the error signal with the triangular waveform. The slope of the inductor-current feedback must be less than that of the triangular waveform:

$$\frac{E_d-v_o}{L}\cdot\alpha\cdot k_i<2V_{tpp}\cdot f_{SW}, \tag{10}$$

where V_{tpp} is the peak-peak value of the triangular waveform. Meanwhile, the gain k_i should be selected as large as possible to improve the current tracing.

A design example is given in TABLE II. According to the data listed, the frequency responses of Equations (1) and (2) are shown in Fig. 7 and Fig. 8 respectively. From Fig. 7, the system is stable and the phase margin is larger than 50°. From Fig. 8, the amplitude response is near $1/\beta$ and little phase shift is between $V_o(S)$ and $V_{ref}(S)$ at the frequency of 50Hz, so the output-voltage can well trace the reference. The high resonant-frequency and wide frequency bandwidth ensure the fast dynamic response.

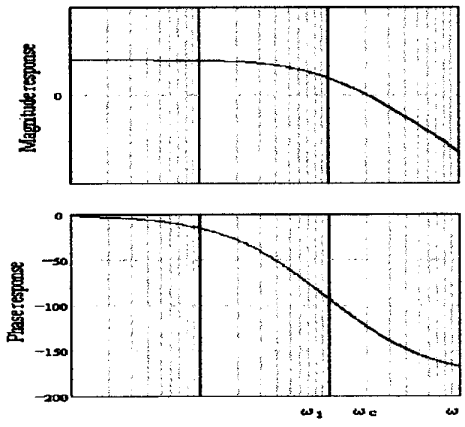

Fig. 6. Magnitude and phase responses of (5)

TABLE II

Specifications And Parameters Of The System

Specifications	Output Capacity	1kVA
	Output voltage	220Vac
	Output Frequency	50Hz
	Input Voltage	±360Vdc
Parameters	Switching Frequency	12.5kHz
	L	4.5mH
	C	5μF
	α	0.46
	β	0.016
	k_m	116
	k_i	2
	k_v	3.75
	τ	0.44ms

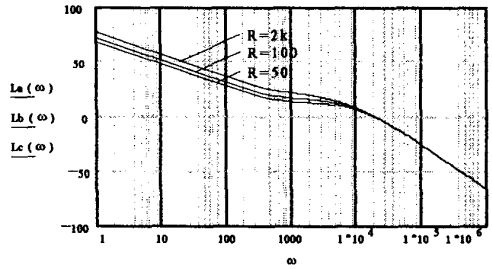

(a) Magnitude response

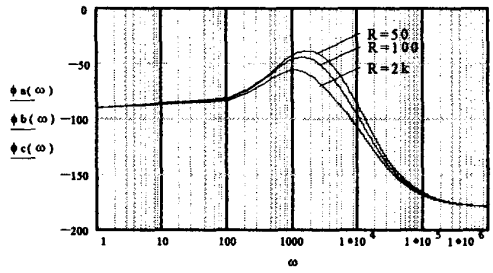

(b) Phase response

Fig. 7. Bode diagram of (1) with given parameters

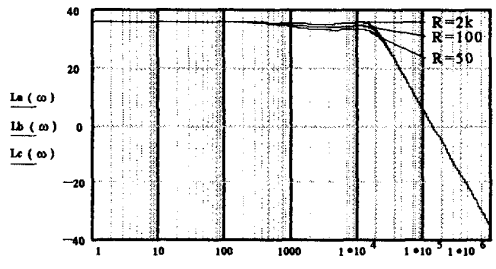

(a) Magnitude response

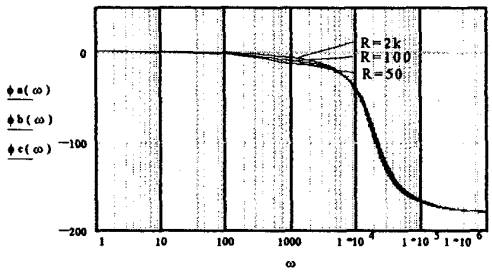

(b) Phase response

Fig. 8. Bode diagram of (2) with given parameters

V. Simulation And Experimental Results

A prototype of 1kVA current-mode controlled voltage-source UPS inverter has been built in laboratory. The specifications and parameters are as listed in TABLE II. Fig. 9–12 and Fig. 13–15 show the simulation and experimental results under resistant load condition respectively.

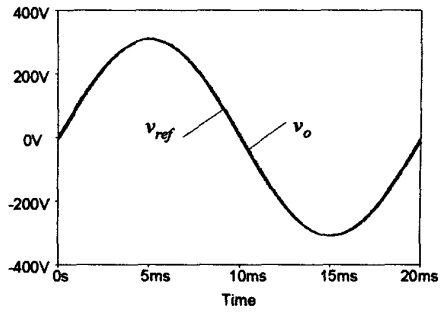

Fig. 9. Simulation results of the steady-state waveform of output-voltage

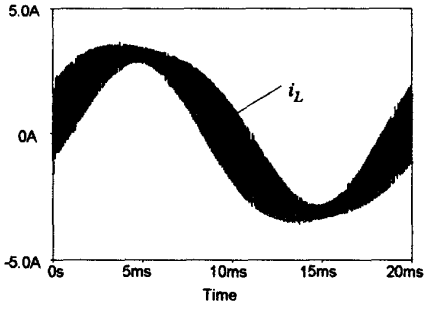

Fig. 10. Simulation results of the steady-state waveform of inductor-current (half load)

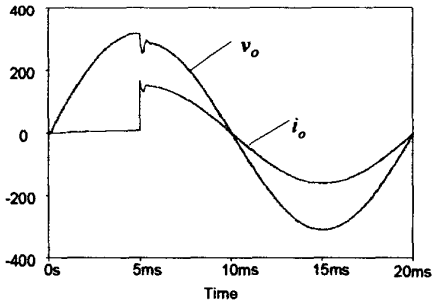

Fig. 11. Simulation results of the dynamic response waveform (no load to half load)

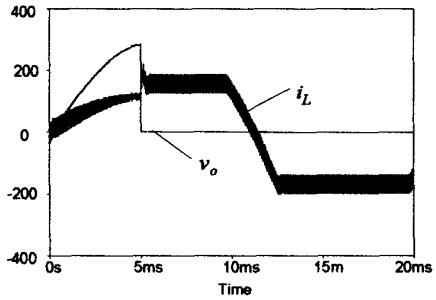

Fig. 12. Simulation results of current limiting under load short

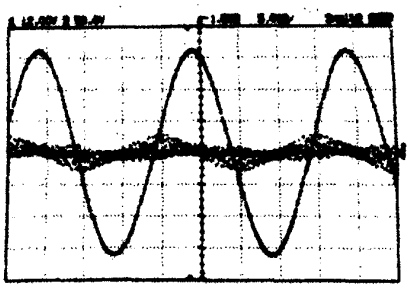

Fig. 13. Experimental results of the output-voltage and inductor-current under no load condition
(voltage=100V/div, current=4A/div)

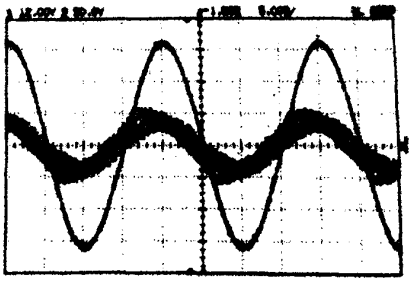

Fig. 14. Experimental results of the output-voltage and inductor-current under half load condition
(voltage=100V/div, current=4A/div)

Fig. 15. Experimental results of the output-voltage and inductor-current under abrupt load change from no load to half load condition
(voltage=100V/div, current=4A/div)

Fig. 9 shows the steady-state waveform of the output-voltage. The output-voltage has a good sinusoidal waveform and very small ripples, and traces well with the reference. The total harmonic distortion of the output-voltage is calculated to be 1.3%.

Fig. 10 shows the inductor-current, which is composed of a low-frequency current and high-frequency ripples. It can be seen that the ripples are limited within a certain band and the largest ripples happen around the zero output-voltage.

The dynamic response to the abrupt load change from no load to half load is shown in Fig. 11. The whole transient time is shorter than 1ms and the output-voltage has a low distortion.

Fig. 12 shows the situation of load short. When load short happens, the output current is limited tightly to a given value. By appropriate designing, the output current can be limited under a safe value.

The experimental results shown in Fig. 13–15 are coincide with the simulation results. Fig. 13 shows the steady-state waveforms of the output-voltage and the inductor-current under no load condition. The inductor-current is sensed with a current transformer. The figure shows the output-voltage is nearly perfectly sinusoidal. The inductor-current is just the filter capacitor-current. Fig. 14 shows the waveforms under half load condition. The inductor-current includes the load-current in addition to the capacitor-current.

Fig. 15 shows the dynamic response to the abrupt load changing. The inductor-current is under perfect control, which contributes to the good performance of the output-voltage.

In the tests of the prototype, the load short experiment has also been accomplished. The output-current can be limited effectively to a safe value for power devices. But this value is still relatively large because it must be larger than rush current under normal operation in actual application. In the experiment this value is measured as 16A. To avoid unnecessary loss, the limit setting should be drawn to zero when load short is detected.

VI. Conclusion

An alternative instantaneous inductor-current controlled SPWM current-mode control technique for voltage-source UPS inverters has been presented, which has the both advantages of current-mode control and SPWM control.

With this control method, not only the output-voltage can be differentially pre-rectified to improve the transient response, but also the output current can be directly controlled. The stability analysis shows that the system performs well from no load to full load, with small over-regulating magnitude and short regulating time against load change. It is confirmed by the simulation and experimental results that the system has an excellent performance with low harmonic distortion in output-voltage, much improved operation stability and reliability, as well as fast dynamic responsibility.

The proposed current-mode control technique can be applied in UPS and all other inverters requiring high performance. It is also attractive for the inherent output current limitation in case of load short and the easy parallel operation and capacity expansion of UPS systems with instantaneous load current sharing.

REFERENCES

[1] D. M. Divan, "Inverter Topologies and Control Techniques for Sinusoidal Output Power Supplies," *IEEE APEC'91 Conf. Rec.*, 1991, pp. 81-86

[2] T. Kagotani, K. Kuroki, J. Shinohara, and A. Misaizu, "A Novel UPS Using High-Frequency Switch-Mode Rectifier and High-Frequency PWM Inverter," *IEEE PESC'89 Conf. Rec.*, 1989, pp. 53-57

[3] A. S. Kislovski, R. Redl, and N. O. Sokal, *Dynamic Analysis of Switching-Mode DC/DC Converters*, Van Nostrand Reinhold, 1991 (ISBN 0-442-23916-5)

[4] M. Carpita, M. Mazzucchelli, S. Savio, and G. Sciutto, "A New PWM Control System for UPS Using Hysteresis Comparator," *IEEE IAS'87 Ann. Meet. Conf. Rec.*, 1987, pp. 749-754

[5] L. Malesani, P. Mattavelli, and P. Tomasin, "Improved Constant-Frequency Hysteresis Current Control of VSI Inverters with Simple Feedforward Bandwidth Prediction," *IEEE Trans. Ind. Applicat.*, vol. 33, no. 5, pp. 1194-1197, Sept./Oct. 1997

[6] L. Malesani and P. Tenti, "A Novel Hysteresis Control Method for Current-Controlled Voltage-Source PWM Inverters with Constant Modulation Frequency," *IEEE Trans. Ind. Applicat.*, vol. 26, no. 1, pp. 88-92, Jan./Feb. 1990

[7] W. Mcmurray, "Modulation of the Chopping Frequency in Dc Choppers and Inverters Having Current-Hysteresis Controllers," *IEEE Trans. Ind. Applicat.*, vol. 20, no. 4, pp. 763-768, July/Aug. 1984

[8] B. K. Bose, "An Adaptive Hysteresis-Band Current Control Technique of a Voltage-Fed PWM Inverter for a Machine Drive System," *IEEE Trans. Ind. Electr.*, Vol. 37, pp. 402-408, Oct. 1990

[9] J. Holtz and S. Stadtfeld, "A Predictive Controller for the Stator Current Vector of ac Machines Fed from a Switched Voltage Source," *IPEC Conf. Rec.*, 1983, pp. 1665-1675

[10] N. M. Abdel-Rahim and J.E. Quaicoe, "Analysis and Design of a Multiple Feedback Loop Control Strategy for Single-Phase Voltage-Source UPS Inverter," *IEEE Trans. Power Elect.*, vol. 11, no. 4, pp. 532-541, July 1996

[11] M. J. Ryan and R. D. Lorenz, "A High Performance Sine Wave Inverter Controller with Capacitor Current Feedback and 'Back-EMF' Decoupling," *IEEE PESC'95 Conf. Rec.*, 1995, pp. 507-513

[12] J. F. Chen and C. L. Chu, "Combination Voltage-Controlled and Current-Controlled PWM Inverters for UPS Parallel Operation," *IEEE Trans. Power Elect.*, vol. 10, no. 5, Sept. 1995, pp. 547-558